Recycling of biomass wastes from amarula husk by a modified facile economical water salt method for high energy density ultracapacitor application

Delvina Japhet Tarimo, Abdulmajid A. Mirghni, Kabir O. Oyedotun, Gift Rutavi, Vianney N. Kitenge and Ncholu Manyala*.

Department of Physics, Institute of Applied Materials, SARChI Chair in Carbon Technology and Materials, University of Pretoria, Pretoria 0028, South Africa.

*Corresponding author's email: ncholu.manyala@up.ac.za, Tel.: + (27)12 420 3549.

HIGHLIGHTS

- Amarula husk (biomass waste) was successfully recycled and transformed into energy storage.
- The approach used is simple, environmentally friendly and cost-efficient.
- The symmetric device demonstrated an outstanding increase in energy density.
- The porous activated carbon has a prominent application for supercapacitor device.

ABSTRACT

In this study, we are reporting for the first time the activated carbon from amarula seed husk (AMH) produced by a modified facile synthesis method producing low-cost, high porosity materials through impregnation of raw materials with water salt. The water salt treatment resulted from the salt formed by a mixture of caclium chloride and phosphoric acid. Calcium influences the catalytic of dehydroxylation and desiccation while phosphate groups stimulates the pyroltic tranformation of the raw material which increases the expansion of pores on the surface of the carbon materials thus prevents destruction of the carbon structure and produce a high yield. The treated AMH with water salt displayed high specific surface area with a maximum specific capacitance of 275 F g^{-1} at 0.5 A g^{-1} in a three-electrode configuration. The fabricated symmetric device presented a specific energy and power of 16 Wh kg^{-1} and 450 W kg^{-1} at 0.5 A g^{-1}, and retained 10 Wh kg^{-1} and 18 kW kg^{-1} at 20 A g^{-1}. The symmetric device retained a capacitance retention of 94.3% noted after 13,000 cycling and 88.5% for up to 20,000

cycling at 5 A g^{-1}. An exceptional increase in specific energy from 15.5 to 38.3 Wh kg^{-1} at 1 A g^{-1} was noted after 200 h floating time. The results propose the potential synthesis progress for recycling and transforming economical biomass waste for developing high performing energy storage device. The approach used in this work is simple and cost-efficient compared to other method that comprises of high temperature and organic chemicals, which are poisonous and corrosive to the environment.

GRAPHICAL ABSTRACT

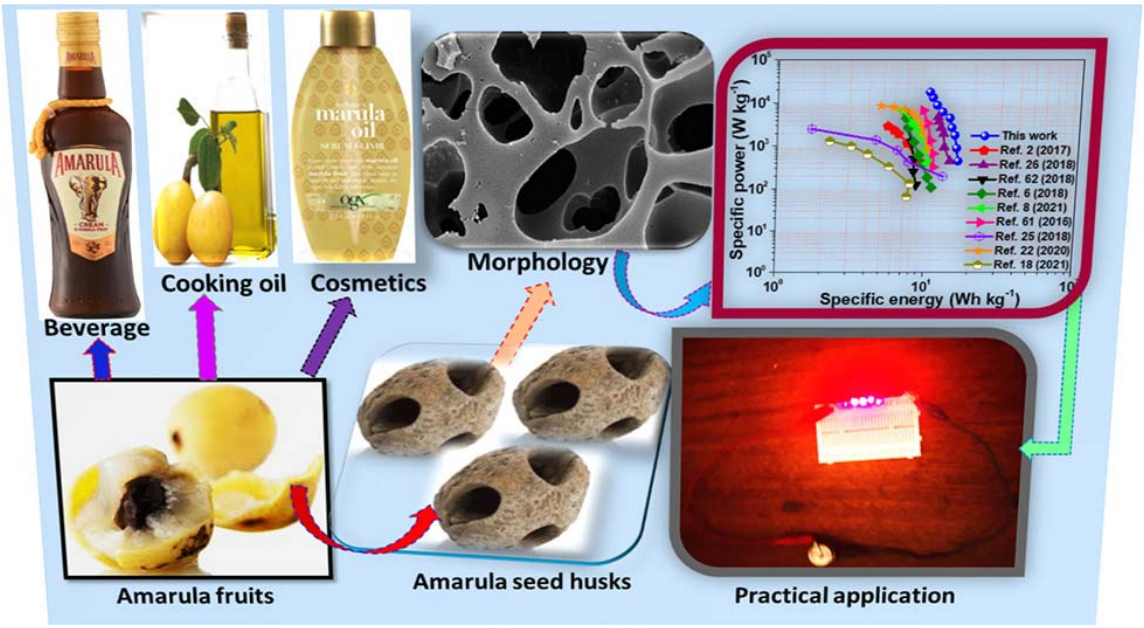

KEYWORDS: Amarula seed husk; Porous activated carbon; Energy storage; Water-salt method; Biomass waste recycling; Supercapacitor.

1. INTRODUCTION

Each year, there is a lot of biomass produced from agriculture which are coverted into food, raw materials and their reminants forms biomass wastes. These wastes are disposed off through burning which discharges sprinkles and air pollution. Thus, inventive approach is required immediately to diminish the opposing effect of burning biomass wastes to the atmospheres [1–

5]. The effects can be reduced by converting biomass wastes into carbon materials that can be used as a source of renewable-energy storage devices like superacacitor, battery and feedstock [6,7]. For the past few decades, a substantial growth in commercialization of supercapacitors has initiated more research activity. This is because supercapacitors have incredible effects on various applications extending from electronics devices to hybrid electric vehicles owing to their outstanding cycling performance, astonishing specific power and greater chemical and thermal stability [8–11].

Supercapacitors are manufactured from carbonaceous materials including 2D materials (e.g. graphene, MXenes), nanoporous carbon (e.g. activated carbon from animal and plant wastes), conducting polymers and metal hydroxides/oxides [12–16]. The carbon materials from biomass wastes have gained a lot of interest owing to astounding conductivity, high specific surface area (SSA), fairly low cost, and their capacitive nature that contribute into an exceptional specific power resulting from the fast charge-discharge abilities [17–20]. This provides an ultimate power basis for electronic application devices like portable computer (laptop) and mobile phones [21,22]. These materials can be produced by a thermochemical procedure which involves physical and chemical activation route [23,24]. Physical activation process involves the pyrolysis of the raw materials in an inert enviroment to eliminate completely the volatile contaminants followed by gasification at high temperature using steam, carbon dioxide or air to open up the closed pores which resulted into a powerful carbon arrangements. The chemical activation process implicates chemical mediators which stimulate pyroltic breakdown causing the development of tar that escalates the carbon yield with a well developed pores. Chemical activation involves one step and lower pyrolysis temperature to produce carbon constituents with high SSA and pore size compared to physical activation. [25–28]. Consequently, chemical activation method has been favored for the production of energy storage materials.

On the other hand, there is no specific method recommended to synthesize activated carbon because the properties of the produced carbon sample are connected with their structure which is resolved by the type of initial raw material, activating agent and condition of pyrolysis procedure [27,29–32]. This shows that each method depends on the compatibility between precursor and the raw material thus produce carbon with different properties [33–35]. In general, the electrochemical performance of supercapacitor is mainly influenced by structures of the electrode constituents. These properties can be improved by synthesis method in which some studies have shown that modification and/or combination of the two methods is efficient for the production of high performing carbon materials [36,37]. For example, Sylla et al. [38] synthesized hierarchically porous activated carbon from peanut shell waste via a two steps (carbonization/activation). They obtained a SSA and specific capacitance of 2547 $m^2 g^{-1}$ and 242.3 F g^{-1} for the optimized sample which is higher than 1481.59 $m^2 g^{-1}$ and 239.88 F g^{-1} obtained by Gue et al. [39] using peanut shell waste via a one step activation process. Usually, a straightforward chemical activation is not highly operational in place of two-step activation, as the previous is concetrated mostly on the surface of the carbon and the inner surface does not react with the activating agent. This is because during the process of carbonization the chemical mediators/agents integrated in the raw materials can decrease the evolution of unstable contaminants and hence hinder the shrinkage of the particles which might have reacted during thermal decomposition. Thus precursor that have been precipitated will release gases and form amorphous structures with pores opening owing to the expirienced condensation and reaction rearrangement [40–42].

Chemical activation can be modified by high-temperature molten salt process that can be utilize in place of a reaction medium for carbon production and/or modification. Previous studies have

reported about the use of high-temperature molten salt to produce carbon materials owing to their low solubility of oxygen and water [21,43–46]. However, the whole process of melting the salt before submerging the raw material into the reactor is complicated and requires high temperature and sometimes longer reaction time, which is not economical and safe for mass production. In this study, the method was modified by a facile procedure consisting of water salt. Water salt is formed when acid and base are mixed together of which both react to neutralize the properties resulting into cation of the acid combines with the anion of the base to form water, while salt is molded by the composite comprising of the base cation and acid anion. This procedure is excellent for synthesis of carbon materials specifically biomass wastes due to its ability to liquefy reactants, stimulate reactions efficiently and elimination of challenging contaminations hence results into a value-added capacitive carbon. It is easy to control the morphology throughout the carbonization procedure. Hence, we recommend as a naive and an informal synthesis procedure to operate due to the low cost, low poisonous, easy separation of water-soluble salts from the products for recycling which confirm affordability and environmental safeguarding. Therefore, should be considered in terms of energy saving and resource sustainability.

Amarula plants are mutual in Sub-saharan countries in Africa. It produces fruits with seed inside which have been used for various purposes including production of beverage (like alcohol), medicine, cooking oil, cosmetics and jam. Nonetheless, all these products are manufactured from amarula plants, fruits and seed, while the seed husk been castoff as a waste resource, which resulted into ecological contamination. This study report for the first time the use of amarula seed husk (AMH) as a potential resource for supercapacitor application through a modified facile, simple and low-cost process via impregnation of biomass wastes with water salt accompany by carbonization/activation. The water salt treatment resulted from the salt formed by a mixture of caclium chloride and phosphoric acid. The treated AMH using water salt demonstrated higher

SSA of 1672 m^2/g as equated to 857 m^2/g of the untreated AMH. The treated AMH sample appeared to display enhanced electrochemical performance with a specific capacitance of 275 and 149 F g^{-1} at 0.5 A g^{-1} recorded in the negative and positive potential windows, respectively. The invented symmetric device demonstrated an excellent specific energy of 38.3 Wh kg^{-1} at 1 A g^{-1} distinguished after 200 h floating time. The symmetric device presented a slight capacitance loss, at 5 A g^{-1} only 5.7% (94.3% preserved) recorded for 13,000 cycling and 14.7% (88.3% conserved) for up to 20,000 cycling. The modified facile synthesis process used in this study is straightforward and economical in comparison with other method, which includes high temperature, and organic chemicals that are toxic and caustic. The results offer a standpoint for adopting the synthesis route and porous activated carbon from AMH for developing a supercapacitor, which has improvement to the current state of art in energy-storage devices.

2. EXPERIMENTAL INFORMATION

2.1 Production of amarula seed husks (AMH) material

Amarula fruits were bought from the street market in Gauteng province of South Africa. The amarula seed husks (AMH) were collected after consuming the fruits plus the seeds (scheme 1). The husks were washed thorougly with deonized water (DI) and ethanol to get rid of any contaminants and then dried at 80 ^oC for 12 h. 1 g each of calcium cloride and phosphoric acid together were dissolved into 70 ml of DI water and stirred for 20 min before soaking 10 g of AMH into the mixture. The role of calcium cloride and phosphoric acid will be detailed later in the results and discussion part (micrographs section 3.1). The combination was conveyed into autoclave and boiled at 150 ^oC for 12 h to allow the raw material to interact well with the mixture. The recoverd yields was cooled naturally to room temperature, washed till getting a neutral pH followed by drying for 12 h at 80 ^oC. The dried products was mixed with potasium hydroxide in a mass ratio of 1:1, tailed by addition of few drops of water to foam a solid slab

which was carbonized and activated at 700 ºC (5 ºC/min) for 2 h under argon (300 sccm) eviroment. The 700 ºC was adopted as the appropriate temperature to obtain AC from AMH sample as shown in Fig. 4a. The recovered sample was treated with 3 M HCl and DI water till pH value, and dried at 60 ºC for 12 h and named as treated AMH (AMH-TR). For comparison purpose another sample named untreated AMH (AMH-UN) was prepared by direct activation without dissolving the raw material into the mixture of calcium cloride and phosphoric acid.

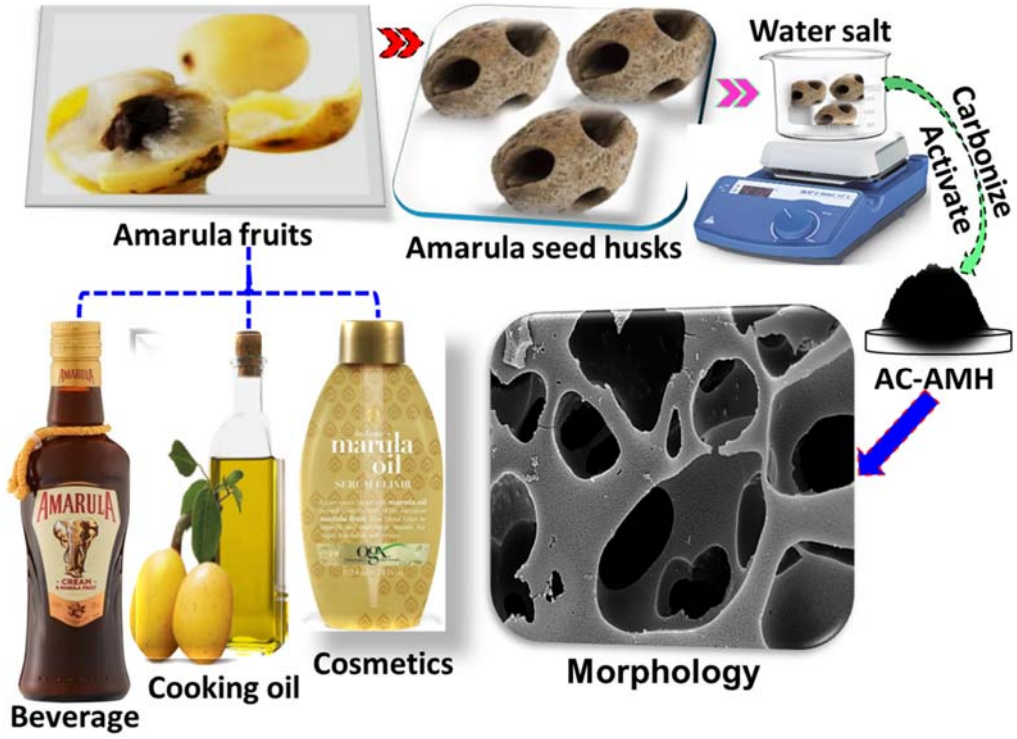

Scheme 1: Schematic illustrations of the synthesis of amarula seed husks (AMH) wastes.

2.2 Material characterization

The micrographs of the treated and untreated AMH samples were obtained using field emission scanning electron microscope functioned at 2.0 kV (Akishima-shi, Japan) equipped with an energy-dispersive spectroscopy (EDS) for the analysis of elemental compositions. The high-

resolution transmission electron micrographs were performed by HR-TEM FEI Tecnai-F30; Akishima-shi, Japan operated at 1.0 kV. The degree of defects in both samples was determined by 532 nm laser wavelength with 5 mW power and 150 s spectra accumulation time via a WITec Confocal Raman Microscope (WITec alpha 300 RAS+ confocal micro-Raman Spectrometer, Ulm-Germany). The phase structure of the synthesized samples was obtained by X-ray diffraction (Bruker BV 2D PHASER); (PANalytical BV, Amsterdam, Netherland) run by a Cu K_{α_1} radiation source ($\lambda = 0.15406\, nm$) by a 30 mA and 50 kV in a step size of 0.05° through a reflection geometry of 2θ values (5 - 90°). The NOVA Touch LX^6 version fitted out using a quanta-chrome Touch-Win software (NOVA touch NT 2 LX-1, 220 V, USA) was utilized to study the nitrogen adsorption-desorption isotherms. The samples were degassed in vacuum for 10 hours run through 150 °C. The relative pressure range (P/Po) of 0.05-0.95 was used in the adsorption division with the aid of Brunauer-Emmett-Teller (BET) method to calculate the SSA while the pore size distribution was determined by density functional theory (DFT).

2.3 Investigation of the electrochemical performance

Three and two electrode arrangements were obtained by VMP300 Bio-Logic potentiostat (Knoxville TN, USA) run in a V11.33 software from the EC-Lab. The electrodes were fabricated by combining the conductive carbon acetylene, polyvinylidene fluoride and active material in the mass ratio of 8:1:1. Thereafter, 1-methyl 2-pyrollidone was mixed to the combination to form slurry that coated onto a nickel form 1.0 x 1.0 cm^2 and a circular diameter of 1.5 cm both with 16 mm thickness before dried for 12 h at 60 °C. The nickel foam was employed as a current collector for three and two-electrode set-up in aqueous 2.5 M KNO_3 electrolyte, respectively.

For three-electrode evaluation; Ag/AgCl, glassy carbon and the synthesized samples with 3.0 mg/cm^2 were applied as a reference, counter and working electrode, respectively. For two-electrode evaluation, a coin-cell type arrangement by the use of fiberglass filter separator

(Whatmann GF/F) sandwiched with active material was used to fabricate the symmetric device. The produced electrodes were tested using cyclic voltammetry (CV) at various scan rates, galvanostatic charge discharge (GCD) at different specific current and electrochemical impedance spectroscopy (EIS) operated in a frequency range 10 mHz – 100 kHz through an open circuit potential of 0.0 V.

The half-cell specific capacitance (C_s) and a single electrode (C_{el}) in the symmetric device was evaluated using the following expressions [47]:

$$C_s = \frac{I_d \times \Delta t}{m_s \times \Delta V} \text{ [F g}^{-1}\text{]} \quad (1)$$

$$C_{el} = 4 \times \left(\frac{I_d \times \Delta t}{m_{tot} \times \Delta V}\right) \text{ [F g}^{-1}\text{]} \quad (2)$$

where, I_d - discharge current in (mA), Δt (s) - time used for an electrode to discharge, m_s - mass loading of the active material in (mg) in a half-cell, m_{tot} mass loading (positive and negative electrode) of the active material in (mg) in a device/full-cell and ΔV - working potential window in (V).

The columbic efficiency C_E (%) was evaluated using the following equation:

$$C_E = \frac{t_D}{t_c} \times 100\% \quad (3)$$

where t_c and t_D presents charge and discharge time.

Since positive and negative electrode displayed different working potential, and different time for charge-discharge then, the mass balance equation is required to balance the charges in the symmetric device. Thus, the followed equation was employed to balance the charges [48]:

$$\frac{m_+}{m_-} = \frac{C_{s-} \times \Delta V_-}{C_{s+} \times \Delta V_+} \quad (4)$$

Followed the above equation, positive and negative electrode masses were evaluated and providing a ratio of 1.0:2.0 resulting in overall mass of the device as 4.2 mg/cm^2.

The specific energy and power of the symmetric device was calculated via the following equations [49]:

$$E_d = \frac{C_{el}(\Delta V)^2}{28.8} \text{ [Wh kg}^{-1}\text{]} \quad (5)$$

$$P_d = \frac{E_d}{\Delta t} \times 3600 \text{ [W kg}^{-1}\text{]} \quad (6)$$

where, E_d and P_d present specific energy and power.

3. RESULTS AND DISCUSSIONS

3.1 Micrographs analysis

The surface morphology of the activated carbon (AC) for untreated and treated amarula seed husk (AMH) obtained via SEM imaging is presented in figure 1. The AMH reveals a grainy roughness with an intersected heterogenous surface and a mixture of randomly distributed cavities. The SEM imaging at low and high magnification of the untreated AMH sample is presented in Fig. 1 (a, b) which shows less porous structures with a closed cavities. After water salt treatment (the salt formed by mixture of caclium chloride and phosphorica acid), the treated AMH morphology become more porous with an open cavities as it can be observed in low and high magnification of Fig. 1 (c, d). The produced nanoporous arrangements in the treated AMH sample are intersected through pores prevailing in the interstitial sites. The formation of interstitial sites results from the decomposition of biomass with water salts whereby moistness and other organic contaminants become released from the compound and the enduring carbonized materials produce the observed morphology. Furthermore, the use of water salt consisting of calcium cloride influences the catalytic of dehydroxylation and desiccation throughout sythesis that pressurize hydrogen and oxygen within the raw material discharge in form of vapour and hence results in the porous structure [6], while phosphoric acid stimulates the pyroltic tranformation of the raw material and contribute in the establishment of the crosslinked structure of the carbon-based material [7]. Also, the phoshate groups from phosphoric acid increases the expansion of pores in an extended state on the surface of the carbon materials thus prevents destruction of the carbon structure and produce a high yield. This was also noted during synthesis whereby less than 10% loss was

recorded from the initial material. This further confirms that the opening of the cavities in the treated AMH with water salt is expexted to display higher SSA and an enhanced electrochemical performance compared to the untreated AMH sample.

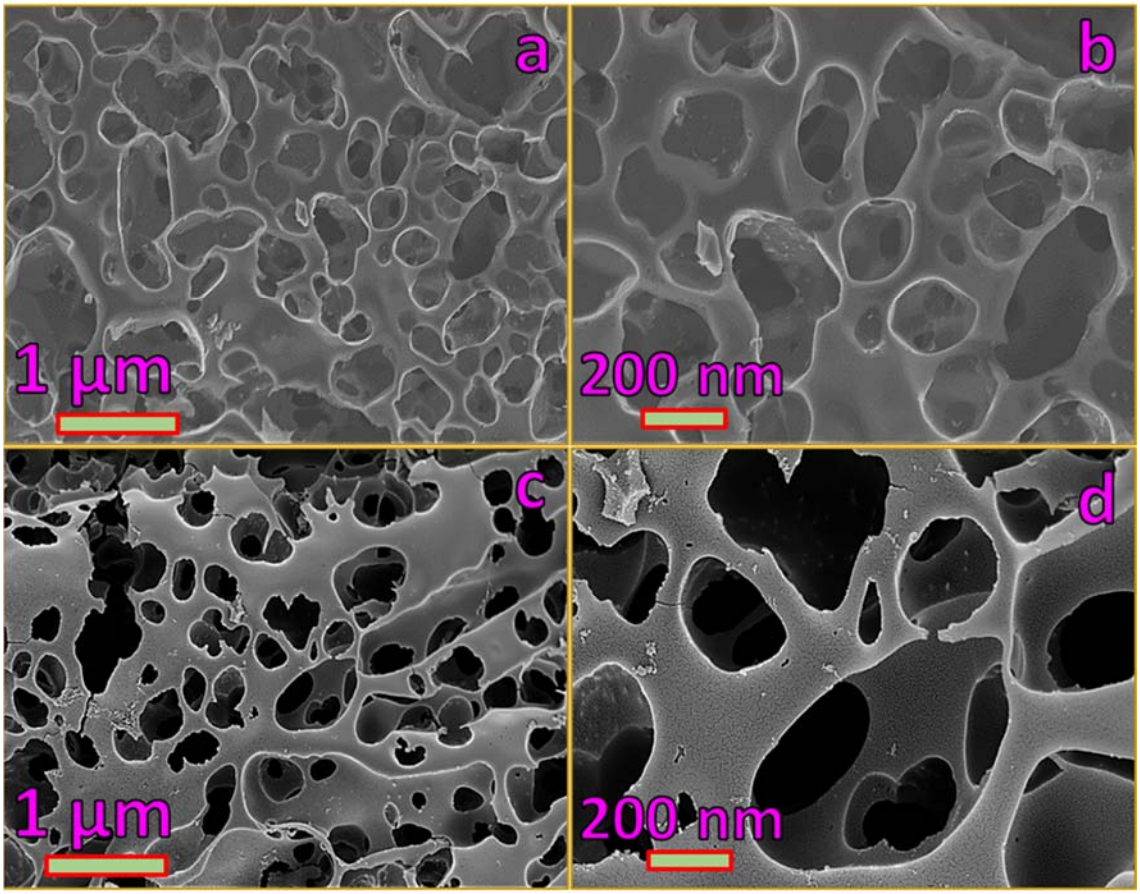

Figure 1: SEM images: (a, b) and (c, d) present low and high magnifications of untreated and treated AMH samples, respectively.

Figure 2 demonstrates the TEM micrographs and EDS elemental analysis of the untreated and treated amarula seed husks (AMH) samples. The TEM images (Fig. 2(a, b)) further confirms the SEM morphology observed in Fig. 1, however the treated AMH sample reveals a clear highly intersected open cavities. The presence of the open cavities is credited to the water salt method adopted during synthesis for this particular sample. The elemental composition was

confirmed by EDS analysis as shown in Fig. 2(c, d) for both samples. The inset to Fig. 2d shows higher amount of carbon (C) content of about 87.91% for the treated AMH sample compared to 80.72% for the untreated AMH (Fig. 2c). The use of water salt method allows the penetration of salt into the structure of the raw materials and permits the release of any contaminants which might block the pores and hence resulted into an open cavities and high carbon content which is ideal for good electrochemical performance.

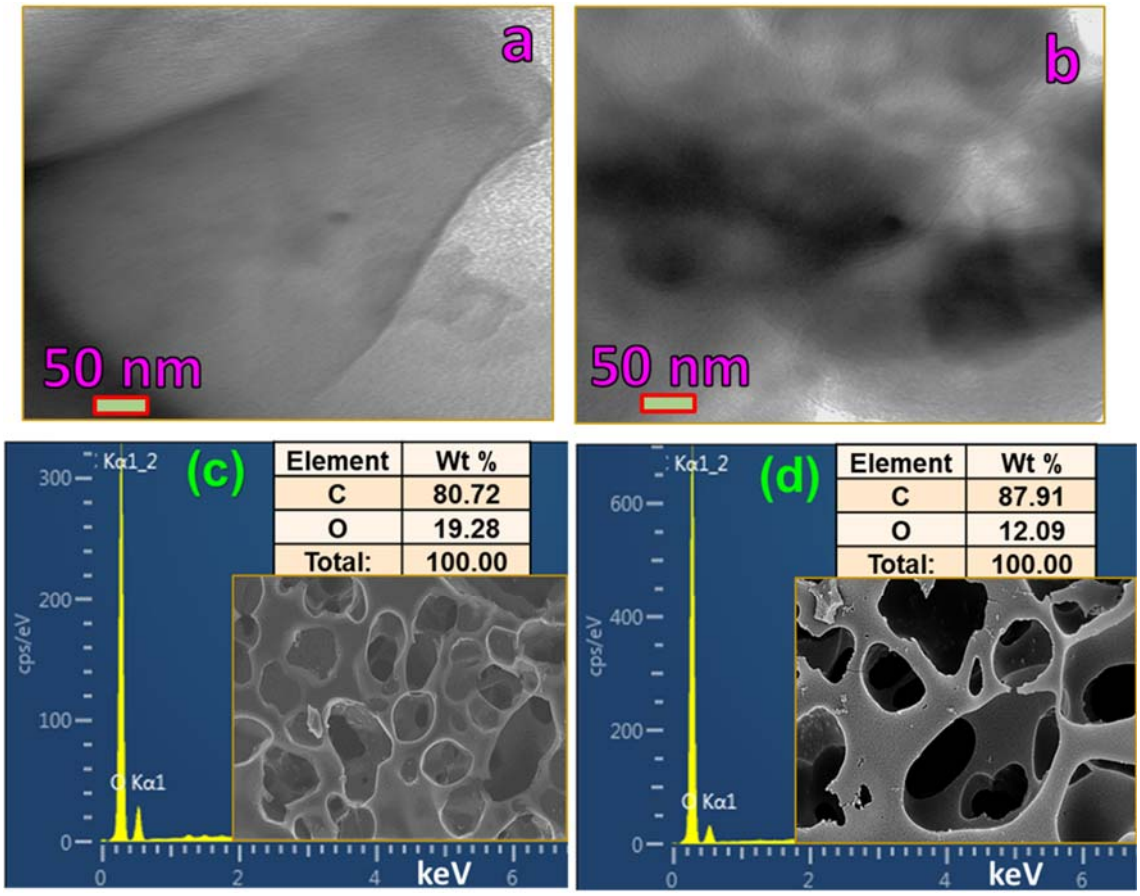

Figure 2: (a, b) TEM images and (c, d) EDS elemental analysis of untreated and treated AMH samples, respectively.

3.2 Structural and BET surface area analysis

Figure 3a displays the Raman spectra of the treated and untreated AMH samples. Three characteristic peaks recognised to D, G and 2D bands of carbon structures are display in both samples. The D band positioned at 1362 cm^{-1} turn out to be active merely in the existence of disorder while the G band located at 1614 cm^{-1} reveal the occurrence of sp^2 hybridized carbon arrangements [50]. The appearance of 2D band at 2886 cm^{-1} reflects the overtones and mixtures of the first order and associated band originated from double resonance phenomenon [51,52]. Correspondingly, it was also noted that D, G and 2D band preserved the similar point, however the intensity of the treated AMH sample is higher compare to the untreated sample suggesting the synergetic effect between AMH and water salt. This further confirms that the AMH sample treated with water salt has more disordered carbon structures. The XRD spectrum of the synthesized treated and untreated AMH samples is shown in figure 3b demonstrating a reduced amount of crystallinity in both samples. In both spectra, the three broad peaks appear at 10^o, 28^o and 43^o assigned to 001, 002 and 100 planes, respectively. The occurrence of 100 plane specifies the growth of upper degree of interlayer condensation of graphite [53] while 002 shows the formation of turbostratic carbon representing the amorphous nature and low degree of graphitization [54]. The trivial divergence of peak intensity and width proposes a well-developed amorphous structures and additional disordered arrangements for the AMH sample treated with water salt in accordance with the Raman results.

The N_2 adsorption and desorption isotherms of the treated and untreated AMH samples are displayed in Fig. 3c. According to the IUPAC grouping system, the presence of micropores and mesopores were noted from the two isotherms suggesting type I isotherms with H4 hysteresis loops [55]. The hysteresis loop of the sample treated with water salt dismisses at lower relative pressure than untreated sample signifying additional micropores in the treated sample [56]. The

BET SSAs are 1672 m^2/g and 857 m^2/g for treated and untreated AMH samples, respectively of which the SSA has doubled for the treated AMH sample. The higher BET specific surface area for the treated AMH sample with water salt is also confirmed by open cavities of the SEM morphology and Raman intensity. Fig. 3d illustrates the pores size distribution for both samples whereby the treated AMH has larger number of pore volume (0.8380 cc/g) compared to the untreated AMH (0.4341 cc/g). This is influenced by the intercalation of water salt molecules in the carbon matrix of AMH.

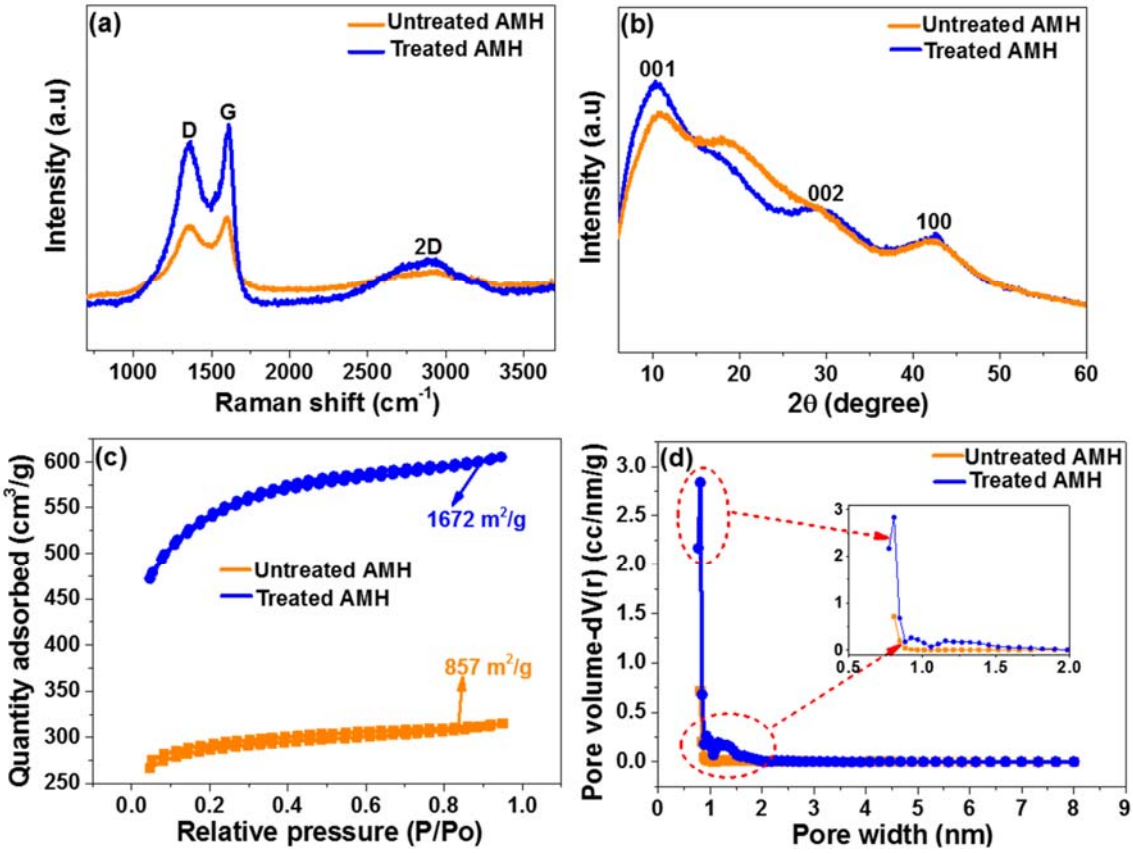

Figure 3: (a) Raman, (b) XRD spectrum, (c) N_2 adsorption – desorption isotherms and (d) pore size distribution of untreated and treated AMH samples, respectively.

3.3 Electrochemical performance analysis

3.3.1 Three-electrode evaluations

The three-electrode set up was employed to evaluate the electrochemical behaviour of the produced sample whereby the treated AMH sample was first used as a control to obtain the actual temperature and electrolyte for this particular material. The effective temperature to obtain the AC from AMH was determined as shown in Fig. 4a in which 700 ^{o}C was found to display higher current response in the CV curves for both potential windows. The electrolyte was optimized as shown in Fig. 4b and the 2.5 M KNO_3 neutral electrolyte outperformed other electrolytes tested. This reveals that the size of the ions in the KNO_3 (K^+ and NO_3^- ions) are suitable to be transported within the pores of the as-synthesized AMH sample [57]. Thus, 700 ^{o}C and 2.5 M KNO_3 was selected for further analysis. Fig. 4a shows the CV profiles at 50 mV s^{-1} for the treated and untreated AMH samples in positive and negative potential windows range of 0.0 to 0.75 V vs Ag/AgCl and -0.9 to 0.0 V vs Ag/AgCl. The CV curves in both potential windows display the ideal rectangular shapes (EDLC behaviour) which presents carbon material's characteristics. It was observed that the CV curve of the treated AMH sample has higher current response in both potential windows. The GCD curves for both samples represented by Fig. 4b within a positive and negative potential window at 1 A g^{-1} display a triangular linear charge-discharge curves, which match with the CV curves in Fig. 4a. Further observation was noted on the treated AMH sample with longer discharge time in contrast to the untreated AMH sample, which agrees with the current response in the CV profiles and confirming that this sample has higher volume of charge storage. The EIS Nyquist plots showing the frequency features for treated and untreated AMH samples in the frequency range 10 mHz – 100 kHz as displayed in Fig. 4c. Consistently, small equivalent series resistance (ESR) value of 0.8 Ω was recorded for the treated AMH compared to 1.1 Ω for the untreated AMH as shown in an insert of Fig. 4c. This indicates good electrical conductivity and small charge transfer resistance of the treated AMH sample compared

to the untreated sample. Furthermore, the treated sample exhibit shorter diffusion length revealing fast ion diffusion at the electrode/electrolyte interface compared to the untreated sample. In general, the treated AMH sample with water salt confirms the enhanced electrochemical performance compared to the untreated sample, which corresponds to the high specific surface area as displayed in Fig. 3c. In addition, Raman data in Fig. 3a further confirms the enhanced electrochemical performance of the treated AMH sample due to the existence of the adequate degree of graphitization with a higher intensity of G band. This shows that a sample with a high number of defects has higher hydrophilicity to the electrolyte ions. Therefore, the existence of ions in water salt is supportive in speeding up the procedure for breaking the chemical bonds among precursors and engineering the surface chemistry of the carbon materials [58].

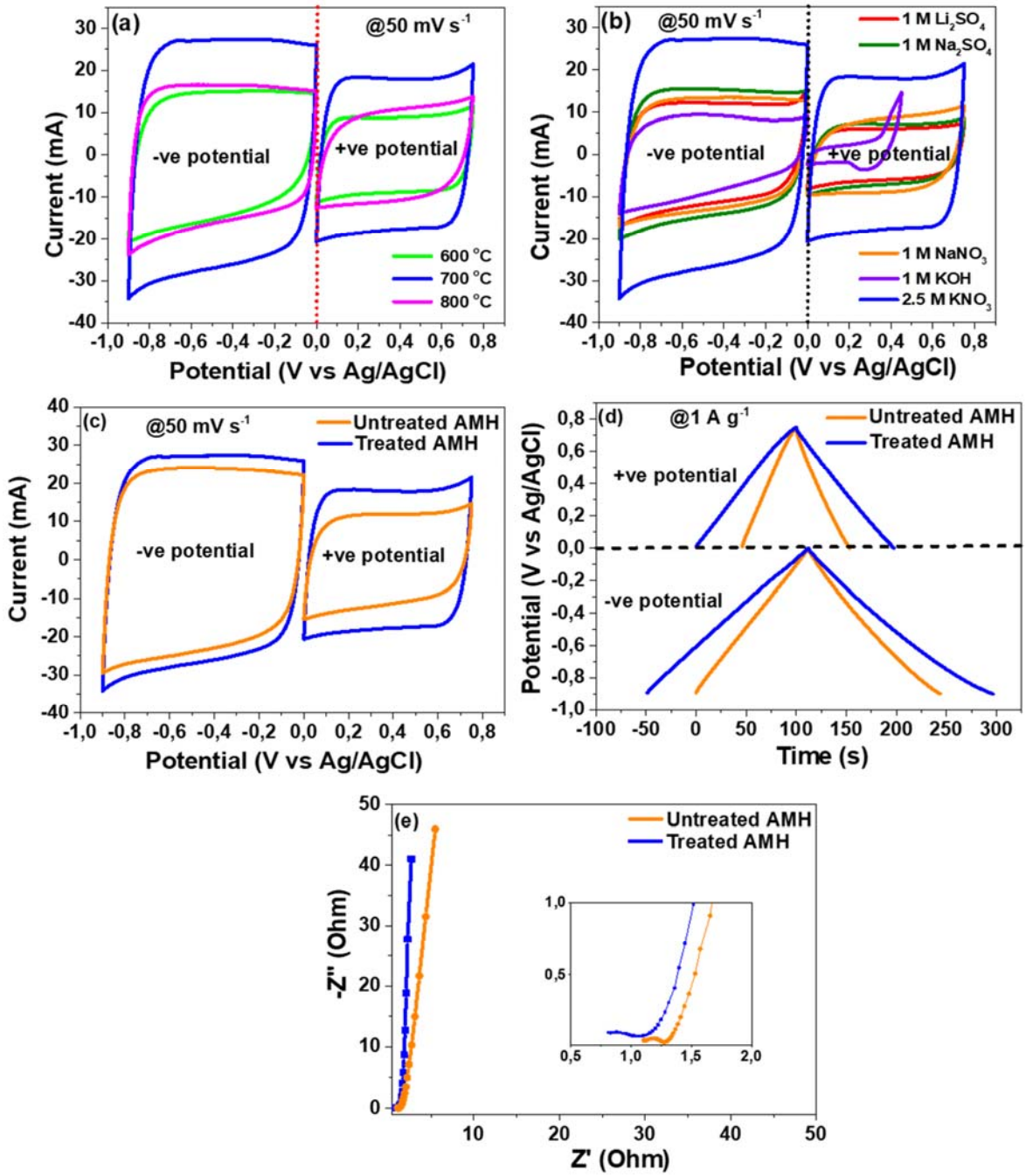

Figure 4: (a) CV curves at a scan rate of 50 mV s^{-1} for treated AMH sample at different temperature using 2.5 M KNO_3 electrolyte and (b) CV curves at 50 mV s^{-1} for treated AMH sample at different electrolytes. (c) CV curves at 50 mV s^{-1}, (d) GCD curves at a specific current of 1 A g^{-1} and (e) EIS Nyquist plot of untreated and treated AMH sample using 700 ºC and 2.5 M KNO_3 electrolyte, respectively.

Fig. 5 shows the detailed electrochemical measurements of the treated sample that presented a superior behaviour as compared to the untreated one. The CV curves presented in Fig. 5 (a, b) showing various scan rates range of 5-100 mV s^{-1} of the treated AMH sample within a potential windows range 0.0-0.75 and -0.9-0.0 V vs Ag/AgCl indicate an ideal rectangular shape presenting distinctive features of EDLC behaviour. Fig. 5 (c, d) displays the GCD curves on different specific currents with the range 0.5-10 A g^{-1} for the treated AMH sample in a similar working potential of the CV curves (Fig. 5 (a, b)). The symmetric triangular characteristics of the GCD profiles indicate the capacitive behaviour of this electrode in both potentials. The specific capacitance (C_s) at different specific currents in both potentials was evaluated using equation 1 and presented by Fig. 5e. The maximum specific capacitance in a negative potential was 275 F g^{-1} while positive potential recorded 149 F g^{-1} both established at 0.5 A g^{-1}. The sample demonstrated good rate capability from 0.5 to 10 A g^{-1} in both potential windows. This performance is influenced by wettability which might be developed by the physical defects and the disordered carbon [59]. Fig. 5f shows the experimental and the fitting EIS Nyquist plot of AMH sample presenting a straight line parallel to the imaginary axis (-Z'' axis) at low frequency region confirming the capacitive behaviour of the sample. The inset to figure Fig. 5f shows the circuit used to fit the EIS data attained from the EC-lab 10.40 by a Z fit software. R1 and R2 stands for equivalent series resistance and charge transfer resistance while C2 and C3 represent the real as well as mass capacitance, respectively. The fitting values for R1 and R2 are 1.0 Ω and 0.7 Ω, which are similar to the experimental values of 0.8 Ω and 0.9 Ω. These low values are attribute of the material's conductivity and short length diffusion associated with the sufficient pore opening as observed in the SEM morphology of Fig. 1 (c, d).

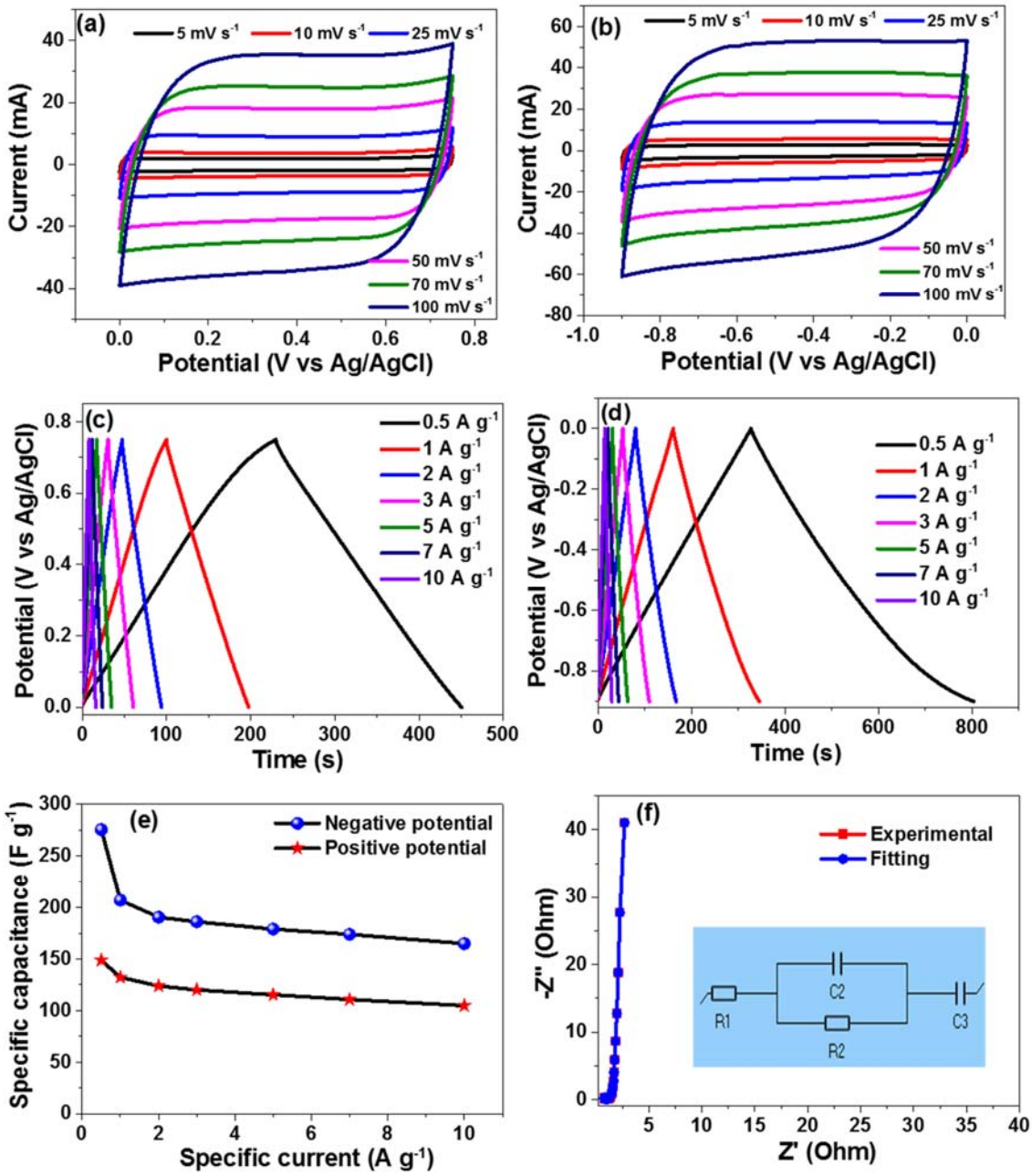

Figure 5: (a, b) and (c, d) present the CV curves at different scan rates and GCD curves at different specific currents in a positive and negative potential window, respectively, (e) Specific capacitance against specific current and (f) EIS Nyquist plot with an inset of equivalent circuit used for EIS fitting of the treated AMH sample.

The enhanced electrochemical performance established by the treated AMH sample stands as a ground for developing a symmetric device (AMH-TR//AMH-TR) in a two-electrode set-up

by utilizing 2.5 M KNO_3 aqueous electrolyte. The balancing of the positive and negative electrode masses was done as demonstrated in equation 4 to balance their charges. This was conducted owing to the difference in potential windows and the charge/discharge rates. Fig. 6a display the CV profiles of the symmetric device at various scan rates range 5 - 100 mV s^{-1} showing the EDLC behaviour. The EDLC features retained even at high scan rates (Fig. 6b) which indicates good rate capability of the sample. The combination of a positive electrode (0.0 to 0.75 V vs Ag/AgCl) and negative electrode (-0.9 to 0.0 V vs Ag/AgCl) in a symmetric device was estimated to have a cell potential of 1.65 V, however, a remarkable increase in a cell potential to 1.8 V was noted. This is aided by the porous nature of the material, high conductivity of the material and 2.5 M KNO_3 neutral aqueous electrolyte which has high ionic concertation and broader operating voltage window [48,60]. The GCD profiles of the AMH-TR//AMH-TR symmetric device at different specific currents from 0.5 - 20 A g^{-1} in Fig. 6c corroborates well with the CV profiles in Fig. 6a. The single electrode specific capacitance in the symmetric device (C_{el}) was evaluated from the GCD profiles at different specific current using equation 2 as observed in Fig. 6d. The highest C_{el} of 140 F g^{-1} was recorded at 0.5 A g^{-1} and retained 89 F g^{-1} at high specific current of 20 A g^{-1} which is equivalent to 64% of the initial capacitance indicating that the device has good rate capability.

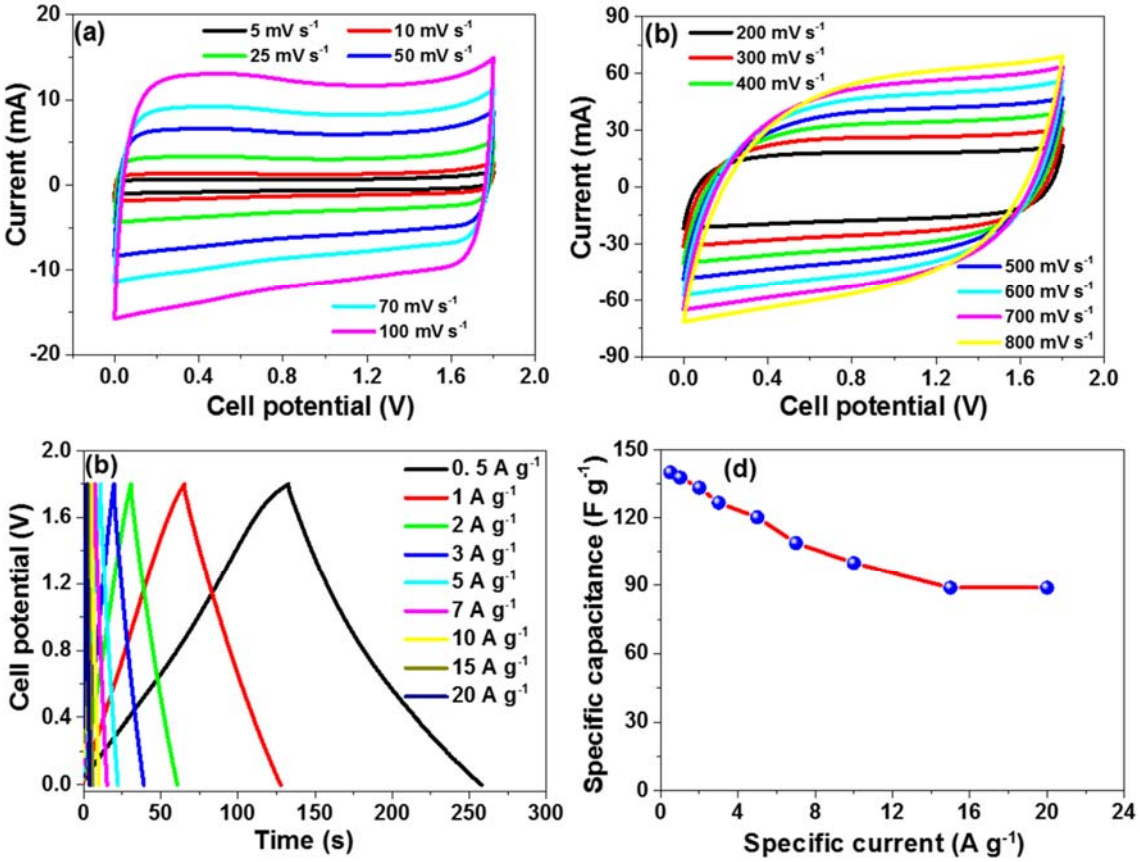

Figure 6: (a, b) stands for CV profiles at low and high scan rates, (c) GCD profiles at different specific currents and (d) specific capacitance versus specific current for AMH-TR//AMH-TR symmetric device.

Fig. 7a shows the Ragone plot of the AMH-TR//AMH-TR symmetric device indicating specific power versus specific energy used to evaluate the potential suitability of a real application. The values for specific energy plus specific power were obtained via equation 5 and 6. The maximum energy and power recorded at 0.5 A g^{-1} were 16 Wh kg^{-1} and 450 W kg^{-1}, respectively and about 10 Wh kg^{-1} and 18 kW kg^{-1} was retained at a maximum specific current of 20 A g^{-1} (Ragone plot this work (a)). The values shown by AMH-TR//AMH-TR symmetric device are substantial higher and ascertained better development of this material towards the existing state-of-art in supercapacitor applications than the recently reported symmetric devices from biomass resources especially lignin/husks/shells in aqueous electrolyte as displayed in the

Ragone plot (Fig. 7a) and table 1 [2,6,8,18,22,25,26,61,62]. The symmetric device also presented a superior columbic efficiency after 20,000 cycling of about 99.9% that is equivalent to 100% at 5 A g^{-1}. An outstanding value of 94.3% capacitance retention was maintained up to 13,000 cycling and 88.5% after 20,000 cycling. The observed performance of 94.3% capacitance retention is attribute to the porous nature of the treated AMH sample, which ease the diffusion of electrolyte ions and hence facilitate the charge/discharge for many numbers of cycles [63]. The sharp drop in capacitance observed at around 13,000 cycles of cycling test was due to the electrochemical degradation of the electrode material as an effect of many cycling. Still, the device was observed to become stable around 14,000 cycles and maintained this steady state for over 20,000 cycles.

Fig. 7c shows the EIS Nyquist plot before and after 20,000 cycling stability as well as after 200 h floating time whereby both plots display similar capacitive behaviour, however, a small deviation from the curve being parallel to the y-axis was noticed after voltage holding. The ESR evaluated on the intercept of the real axis (Z' axis) was found to be 0.57 Ω before 20,000 cycling, and increased a bit higher to 3.81 Ω after 20,000 cycling. Further improvement noted on the reduced diffusion length and ESR of up to 1.9 Ω after subjecting the device to 200 h floating time. This progress was also witnessed in the CV curves of Fig. 7d with enhanced current response after 200 h floating time. This progress signify that the material has become more accessible to the electrolyte ions after 200 h floating time due to the enhanced wettability. Fig. 7e illustrates specific capacitance versus floating time with an inset to the figure presenting charge/discharge profiles whereby an improved in specific capacitance at 1 A g^{-1} from 138 to 340 F g^{-1} after 200 h floating time was noted. This corresponds to an increase in specific energy from 15.5 to 38.3 W kg^{-1} at the same specific current and also for all the specific currents as indicated in the Ragone plot by blue set of data referred to this work (b). Thereafter, two devices

were connected in series to test the practical application by illuminating five LED bulbs connected in parallel each with a rated voltage of 3 V as shown in Fig. 7f.

Table 1: Evaluations of the specific energy and power of comparable activated carbon from biomass resources via two electrode (full cell) set-up.

Biomass material	**Electrolyte**	**Specific current (A g^{-1})**	**Specific energy (Wh kg^{-1})**	**Specific power (W kg^{-1})**	**Cycling stability**	**Ref.**
Sawdust	6 M KOH	0.5	8.4	250	10,000 (3 A g^{-1})	[2]
Peanut shells	1 M H_2SO_4	0.25	10.8	106.9	10,000 (1 A g^{-1})	[6]
Lignin	2.5 M KNO_3	0.5	10	397	15,000 (5 A g^{-1})	[8]
Cornhusk	50% Sea water	0.5	7.44	324	10,000 (2 A g^{-1})	[18]
Soybean	1 M H_2SO_4	0.1	10	259	10,000 (1 A g^{-1})	[22]
Clover stems	1 M H_2SO_4	0.5	10.7	125	10,000 (5 A g^{-1})	[25]
Quercus suber	3 M KNO_3	0.5	14	450	10,000 (5 A g^{-1})	[26]
Coconut shells	PVA-KOH-CB	0.5	11	325	10,000 (5 A g^{-1})	[61]
Pueraria	6 M KOH	0.5	8.46	123	10,000 (1 A g^{-1})	[62]
Amarula seed husks	**2.5 M KNO_3**	**0.5**	**16**	**450**	**20,000 (5 A g^{-1})**	**This work (a)**
		1	**38.3**	**900**	**200 h floating time**	**This work (b)**

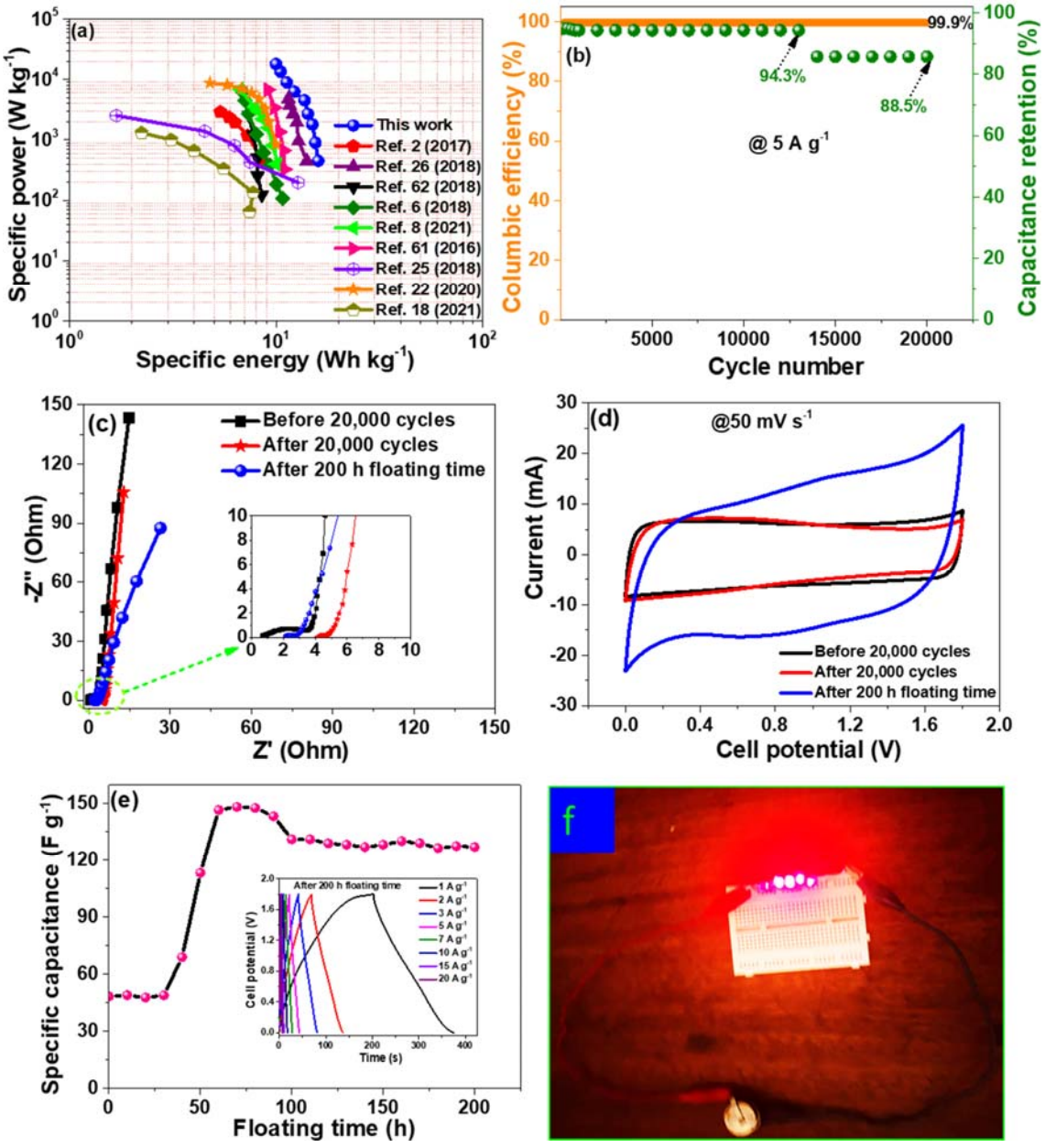

Figure 7: AMH-TR//AMH-TR symmetric device: (a) Ragone plot compared with similar devices in the literature, (b) capacitance retention and columbic efficiency versus cycle number, (c) EIS Nyquist plot before, after 20,000 cycling and after 200 h floating times, (d) CV curves at 50 mV s^{-1} before, after 20,000 cycling and after 200 h floating time, (e) specific capacitance versus floating time with an insert being charge/discharge profiles after 200 h floating time and (f) a snapshot of two devices connected in series used to illuminate five LED bulbs connected in parallel each of 3 V.

4. CONCLUSION

In this study, we have effectively produced and characterized for the first time amarula seed husk (AMH) porous activated carbon through a modified facile and low-cost synthesis process, which turn out to increase the overall electrochemical performance of the synthesized material. The porous carbon was prepared by impregnation of amarula seed husks wastes via water salt and completed by carbonization/activation. The water salt treatment resulted from the salt formed by a mixture of caclium chloride and phosphoric acid. The treated AMH with water salt displayed higher SSA of 1672 m^2/g in comparison to the untreated with 857 m^2/g. The treated AMH sample revealed enhanced electrochemical performance with a specific capacitance of 275 and 149 F g^{-1} established from the negative and positive potential windows at 0.5 A g^{-1}, respectively. The assembled symmetric device has an enhanced cell potential from 1.65 V (combined positive and negative electrode 0.0-0.75 to -0.9-0.0 V vs Ag/AgCl) to 1.8 V owing to the optimized neutral aqueous electrolyte (2.5 M KNO_3). At 0.5 A g^{-1}, the device demonstrated the highest specific capacitance of 140 F g^{-1} which corresponds to the specific energy and power of 16 Wh kg^{-1} and 450 W kg^{-1}, respectively. The symmetric device retained a capacitance retention in which 94.3% recorded for 13,000 cycling and 88.5% for up to 20,000 cycling at 5 A g^{-1}. An excellent rise in specific energy (38.3 Wh kg^{-1}) and power (900 W kg^{-1}) of the device after 200 h floating time was observed indicating a good wettability of the material is confirmed after voltage holding. The modified facile synthesis process employed in this work is simple and cost-effective compared to other approach that involves high temperature and organic chemicals, which are poisonous and corrosive. The outcomes from this study propose the viewpoint for a superior advancement in employing the presented synthesis route and the AC from AMH for prospering the high performing energy storage devices.

ACKNOWLEDGEMENTS

We sincerely acknowledge research support from South African Research Chairs Initiative of the Department of Science and Technology and National Research Foundation of South Africa (Grant No. 61056). Delvina Japhet Tarimo acknowledges the financial support from NRF through SARChI chair in Carbon Technology and Materials.

REFERENCE

[1] A.J. Ding, C.B. Fu, X.Q. Yang, J.N. Sun, T. Petäjä, V.M. Kerminen, T. Wang, Y. Xie, E. Herrmann, L.F. Zheng, W. Nie, Q. Liu, X.L. Wei, M. Kulmala, Intense atmospheric pollution modifies weather: A case of mixed biomass burning with fossil fuel combustion pollution in eastern China, Atmos. Chem. Phys. 13 (2013) 10545–10554. https://doi.org/10.5194/acp-13-10545-2013.

[2] Y. Huang, Y. Liu, G. Zhao, J.Y. Chen, Sustainable activated carbon fiber from sawdust by reactivation for high-performance supercapacitors, J. Mater. Sci. 52 (2017) 478–488. https://doi.org/10.1007/s10853-016-0347-0.

[3] J.G. Lynam, M. Toufiq Reza, V.R. Vasquez, C.J. Coronella, Effect of salt addition on hydrothermal carbonization of lignocellulosic biomass, Fuel. 99 (2012) 271–273. https://doi.org/10.1016/J.FUEL.2012.04.035.

[4] G.M. Kirkelund, C. Magro, P. Guedes, P.E. Jensen, A.B. Ribeiro, L.M. Ottosen, Electrodialytic removal of heavy metals and chloride from municipal solid waste incineration fly ash and air pollution control residue in suspension – test of a new two compartment experimental cell, Electrochim. Acta. 181 (2015) 73–81. https://doi.org/10.1016/J.ELECTACTA.2015.03.192.

[5] V.N. Kitenge, K.O. Oyedotun, O. Fasakin, D.J. Tarimo, N.F. Sylla, X. Van Heerden, N. Manyala, Enhancing the electrochemical properties of a nickel–cobalt-manganese

ternary hydroxide electrode using graphene foam for supercapacitors applications, Mater. Renew. Sustain. Energy. 10 (2021) 1–16. https://doi.org/10.1007/s40243-021-00192-y.

[6] Z. Xiao, W. Chen, K. Liu, P. Cui, D. Zhan, Porous biomass carbon derived from peanut shells as electrode materials with enhanced electrochemical performance for supercapacitors, Int. J. Electrochem. Sci. 13 (2018) 5370–5381. https://doi.org/10.20964/2018.06.54.

[7] M. Zięzio, B. Charmas, K. Jedynak, M. Hawryluk, K. Kucio, Preparation and characterization of activated carbons obtained from the waste materials impregnated with phosphoric acid(V), Appl. Nanosci. 10 (2020) 4703–4716. https://doi.org/10.1007/s13204-020-01419-6.

[8] B.K. Mutuma, N.F. Sylla, A. Bubu, N.M. Ndiaye, C. Santoro, A. Brilloni, F. Poli, N. Manyala, F. Soavi, Valorization of biodigestor plant waste in electrodes for supercapacitors and microbial fuel cells, Electrochim. Acta. 391 (2021) 138960. https://doi.org/10.1016/j.electacta.2021.138960.

[9] P. Veerakumar, T. Maiyalagan, B.G.S. Raj, K. Guruprasad, Z. Jiang, K.C. Lin, Paper flower-derived porous carbons with high-capacitance by chemical and physical activation for sustainable applications, Arab. J. Chem. 13 (2020) 2995–3007. https://doi.org/10.1016/J.ARABJC.2018.08.009.

[10] T. Shang, Y. Xu, P. Li, J. Han, Z. Wu, Y. Tao, Q.H. Yang, A bio-derived sheet-like porous carbon with thin-layer pore walls for ultrahigh-power supercapacitors, Nano Energy. 70 (2020) 104531. https://doi.org/10.1016/J.NANOEN.2020.104531.

[11] L.J. Kennedy, T. Ratnaji, N. Konikkara, J.J. Vijaya, Value added porous carbon from leather wastes as potential supercapacitor electrode using neutral electrolyte, J. Clean. Prod. 197 (2018) 930–936. https://doi.org/10.1016/J.JCLEPRO.2018.06.244.

[12] D.J. Tarimo, K.O. Oyedotun, N.F. Sylla, A.A. Mirghni, N.M. Ndiaye, N. Manyala, Waste chicken bone-derived porous carbon materials as high performance electrode for supercapacitor applications, J. Energy Storage. 51 (2022). https://doi.org/10.1016/j.est.2022.104378.

[13] B.C. Wyatt, B. Anasori, Self-assembly and in-situ characterization of Ti3C2T in Al: A step toward additive manufacturing of MXene-metal composites, Appl. Mater. Today. 27 (2022) 101451. https://doi.org/10.1016/j.apmt.2022.101451.

[14] G. Rutavi, D.J. Tarimo, V.M. Maphiri, N. Manyala, Two-step electrodeposition of Hausmannite sulphur reduced graphene oxide and cobalt-nickel layered double hydroxide heterostructure for high-performance supercapacitor, Int. J. Energy Res. (2022) 1–14. https://doi.org/10.1002/er.7922.

[15] P. Simon, Y. Gogotsi, Perspectives for electrochemical capacitors and related devices, Nat. Mater. 19 (2020) 1151–1163. https://doi.org/10.1038/S41563-020-0747-Z.

[16] C. Wang, B. Yan, J. Zheng, L. Feng, Z. Chen, Q. Zhang, T. Liao, J. Chen, S. Jiang, C. Du, S. He, Recent progress in template-assisted synthesis of porous carbons for supercapacitors, Adv. Powder Mater. 1 (2022) 100018. https://doi.org/10.1016/j.apmate.2021.11.005.

[17] M.A. Azam, N.S.N. Ramli, N.A.N.M. Nor, T.I.T. Nawi, Recent advances in biomass-derived carbon, mesoporous materials, and transition metal nitrides as new electrode materials for supercapacitor: A short review, Int. J. Energy Res. 45 (2021) 8335–8346. https://doi.org/10.1002/er.6377.

[18] C.J. Raj, R. Manikandan, M. Rajesh, P. Sivakumar, H. Jung, S.J. Das, B.C. Kim, Cornhusk mesoporous activated carbon electrodes and seawater electrolyte: The sustainable sources for assembling retainable supercapacitor module, J. Power Sources. 490 (2021) 229518. https://doi.org/10.1016/J.JPOWSOUR.2021.229518.

[19] K. Mahankali, N.K. Thangavel, Y. Ding, S.K. Putatunda, L.M.R. Arava, Interfacial behavior of water-in-salt electrolytes at porous electrodes and its effect on supercapacitor performance, Electrochim. Acta. 326 (2019) 134989. https://doi.org/10.1016/J.ELECTACTA.2019.134989.

[20] K. Li, P. Li, Z. Sun, J. Shi, M. Huang, J. Chen, S. Liu, Z. Shi, H. Wang, All-cellulose-based quasi-solid-state supercapacitor with nitrogen and boron dual-doped carbon electrodes exhibiting high energy density and excellent cyclic stability, Green Energy Environ. (2022). https://doi.org/10.1016/j.gee.2022.01.002.

[21] B. Lu, L. Hu, H. Yin, X. Mao, W. Xiao, D. Wang, Preparation and application of capacitive carbon from bamboo shells by one step molten carbonates carbonization, Int. J. Hydrogen Energy. 41 (2016) 18713–18720. https://doi.org/10.1016/J.IJHYDENE.2016.05.083.

[22] Z. Guo, X. Kong, X. Wu, W. Xing, J. Zhou, Y. Zhao, S. Zhuo, Heteroatom-doped hierarchical porous carbon via molten-salt method for supercapacitors, Electrochim. Acta. 360 (2020) 137022. https://doi.org/10.1016/J.ELECTACTA.2020.137022.

[23] G.S. Dos Reis, S.H. Larsson, H.P. de Oliveira, M. Thyrel, E.C. Lima, Sustainable biomass activated carbons as electrodes for battery and supercapacitors–a mini-review, Nanomaterials. 10 (2020) 1–22. https://doi.org/10.3390/nano10071398.

[24] D. Qiu, C. Kang, A. Gao, Z. Xie, Y. Li, M. Li, F. Wang, R. Yang, Sustainable Low-Temperature Activation to Customize Pore Structure and Heteroatoms of Biomass-Derived Carbon Enabling Unprecedented Durable Supercapacitors, ACS Sustain. Chem. Eng. 7 (2019) 14629–14638. https://doi.org/10.1021/acssuschemeng.9b02425.

[25] C. Wang, D. Wu, H. Wang, Z. Gao, F. Xu, K. Jiang, Biomass derived nitrogen-doped hierarchical porous carbon sheets for supercapacitors with high performance, J. Colloid Interface Sci. 523 (2018) 133–143. https://doi.org/10.1016/j.jcis.2018.03.009.

[26] F.O. Ochai-Ejeh, D.Y. Momodu, M.J. Madito, A.A. Khaleed, K.O. Oyedotun, S.C. Ray, N. Manyala, Nanostructured porous carbons with high rate cycling and floating performance for supercapacitor application, AIP Adv. 8 (2018). https://doi.org/10.1063/1.5023046.

[27] T.M. Alslaibi, I. Abustan, M.A. Ahmad, A.A. Foul, A review: Production of activated carbon from agricultural byproducts via conventional and microwave heating, J. Chem. Technol. Biotechnol. 88 (2013) 1183–1190. https://doi.org/10.1002/jctb.4028.

[28] D.P. Yang, Z. Li, M. Liu, X. Zhang, Y. Chen, H. Xue, E. Ye, R. Luque, Biomass-Derived Carbonaceous Materials: Recent Progress in Synthetic Approaches, Advantages, and Applications, ACS Sustain. Chem. Eng. 7 (2019) 4564–4585. https://doi.org/10.1021/acssuschemeng.8b06030.

[29] J. Pampel, C. Denton, T.P. Fellinger, Glucose derived ionothermal carbons with tailor-made porosity, Carbon N. Y. 107 (2016) 288–296. https://doi.org/10.1016/j.carbon.2016.06.009.

[30] H. Luo, Y. Yang, X. Zhao, J. Zhang, Y. Chen, 3D sponge-like nanoporous carbons via a facile synthesis for high-performance supercapacitors: direct carbonization of tartrate salt, Electrochim. Acta. 169 (2015) 13–21. https://doi.org/10.1016/J.ELECTACTA.2015.04.049.

[31] Z. Wu, J. Zou, Y. Zhang, X. Lin, D. Fry, L. Wang, J. Liu, Lignin-derived hard carbon anode for potassium-ion batteries: Interplay among lignin molecular weight, material structures, and storage mechanisms, Chem. Eng. J. 427 (2022) 131547. https://doi.org/10.1016/j.cej.2021.131547.

[32] B. Krüner, A. Schreiber, A. Tolosa, A. Quade, F. Badaczewski, T. Pfaff, B.M. Smarsly, V. Presser, Nitrogen-containing novolac-derived carbon beads as electrode material for supercapacitors, Carbon N. Y. 132 (2018) 220–231.

https://doi.org/10.1016/j.carbon.2018.02.029.

[33] Z. Bi, Q. Kong, Y. Cao, G. Sun, F. Su, X. Wei, X. Li, A. Ahmad, L. Xie, C.M. Chen, Biomass-derived porous carbon materials with different dimensions for supercapacitor electrodes: A review, J. Mater. Chem. A. 7 (2019) 16028–16045. https://doi.org/10.1039/c9ta04436a.

[34] G. Zhang, T. Guan, N. Wang, J. Wu, J. Wang, J. Qiao, K. Li, Small mesopore engineering of pitch-based porous carbons toward enhanced supercapacitor performance, Chem. Eng. J. 399 (2020) 125818. https://doi.org/10.1016/J.CEJ.2020.125818.

[35] Y. Ge, Z. Liu, Y. Wu, R. Holze, On the utilization of supercapacitor electrode materials, Electrochim. Acta. 366 (2021) 137390. https://doi.org/10.1016/J.ELECTACTA.2020.137390.

[36] M.J. Prauchner, F. Rodríguez-Reinoso, Chemical versus physical activation of coconut shell: A comparative study, Microporous Mesoporous Mater. 152 (2012) 163–171. https://doi.org/10.1016/J.MICROMESO.2011.11.040.

[37] X. Yuan, P.D. Dissanayake, B. Gao, W.J. Liu, K.B. Lee, Y.S. Ok, Review on upgrading organic waste to value-added carbon materials for energy and environmental applications, J. Environ. Manage. 296 (2021) 113128. https://doi.org/10.1016/J.JENVMAN.2021.113128.

[38] N.F. Sylla, N.M. Ndiaye, B.D. Ngom, D. Momodu, M.J. Madito, B.K. Mutuma, N. Manyala, Effect of porosity enhancing agents on the electrochemical performance of high-energy ultracapacitor electrodes derived from peanut shell waste, Sci. Rep. 9 (2019) 1–15. https://doi.org/10.1038/s41598-019-50189-x.

[39] F. Guo, X. Jiang, X. Li, K. Peng, C. Guo, Z. Rao, Carbon electrode material from peanut shell by one-step synthesis for high performance supercapacitor, J. Mater. Sci.

Mater. Electron. 30 (2019) 914–925. https://doi.org/10.1007/s10854-018-0362-9.

[40] F. Amran, M.A.A. Zaini, Effects of chemical activating agents on physical properties of activated carbons – A commentary, Water Pract. Technol. 15 (2020) 854–876. https://doi.org/10.2166/wpt.2020.094.

[41] J. Li, K. Han, J. Qi, Z. Teng, M. Li, M. Wang, Biomass-derived 3D hierarchical porous carbon by two-step activation method for supercapacitor, J. Mater. Sci. Mater. Electron. 30 (2019) 19415–19425. https://doi.org/10.1007/s10854-019-02303-y.

[42] J. Cheng, S.C. Hu, G.T. Sun, K. Kang, M.Q. Zhu, Z.C. Geng, Comparison of activated carbons prepared by one-step and two-step chemical activation process based on cotton stalk for supercapacitors application, Energy. 215 (2021) 119144. https://doi.org/10.1016/J.ENERGY.2020.119144.

[43] D. Tang, Y. Luo, W. Lei, Q. Xiang, W. Ren, W. Song, K. Chen, J. Sun, Hierarchical porous carbon materials derived from waste lentinus edodes by a hybrid hydrothermal and molten salt process for supercapacitor applications, Appl. Surf. Sci. 462 (2018) 862–871. https://doi.org/10.1016/J.APSUSC.2018.08.153.

[44] H. Yin, B. Lu, Y. Xu, D. Tang, X. Mao, W. Xiao, D. Wang, A.N. Alshawabkeh, Harvesting capacitive carbon by carbonization of waste biomass in molten salts, Environ. Sci. Technol. 48 (2014) 8101–8108. https://doi.org/10.1021/es501739v.

[45] A. Rezaei, A.R. Kamali, Green production of carbon nanomaterials in molten salts, mechanisms and applications, Diam. Relat. Mater. 83 (2018) 146–161. https://doi.org/10.1016/J.DIAMOND.2018.02.003.

[46] H. He, L. Zan, J. Liu, Y. Zhang, Template-assisted molten-salt synthesis of hierarchical lithium-rich layered oxide nanowires as high-rate and long-cycling cathode materials, Electrochim. Acta. 333 (2020) 135558. https://doi.org/10.1016/j.electacta.2019.135558.

[47] K.O. Oyedotun, F. Barzegar, A.A. Mirghni, A.A. Khaleed, T.M. Masikhwa, N. Manyala, Examination of High-Porosity Activated Carbon Obtained from Dehydration of White Sugar for Electrochemical Capacitor Applications, ACS Sustain. Chem. Eng. 7 (2019) 537–546. https://doi.org/10.1021/acssuschemeng.8b04080.

[48] D.J. Tarimo, K.O. Oyedotun, A.A. Mirghni, N.F. Sylla, N. Manyala, High energy and excellent stability asymmetric supercapacitor derived from sulphur-reduced graphene oxide/manganese dioxide composite and activated carbon from peanut shell, Electrochim. Acta. 353 (2020) 136498. https://doi.org/10.1016/j.electacta.2020.136498.

[49] A.R. Selvaraj, A. Muthusamy, Inho-Cho, H.J. Kim, K. Senthil, K. Prabakar, Ultrahigh surface area biomass derived 3D hierarchical porous carbon nanosheet electrodes for high energy density supercapacitors, Carbon N. Y. 174 (2021) 463–474. https://doi.org/10.1016/J.CARBON.2020.12.052.

[50] A. Adan-Mas, L. Alcaraz, P. Arévalo-Cid, F.A. López-Gómez, F. Montemor, Coffee-derived activated carbon from second biowaste for supercapacitor applications, Waste Manag. 120 (2021) 280–289. https://doi.org/10.1016/J.WASMAN.2020.11.043.

[51] A. Ghosh, C. do A. Razzino, A. Dasgupta, K. Fujisawa, L.H.S. Vieira, S. Subramanian, R.S. Costa, A.O. Lobo, O.P. Ferreira, J. Robinson, M. Terrones, H. Terrones, B.C. Viana, Structural and electrochemical properties of babassu coconut mesocarp-generated activated carbon and few-layer graphene, Carbon N. Y. 145 (2019) 175–186. https://doi.org/10.1016/J.CARBON.2018.12.114.

[52] D.J. Tarimo, K.O. Oyedotun, A.A. Mirghni, N. Manyala, Sulphur-reduced graphene oxide composite with improved electrochemical performance for supercapacitor applications, Int. J. Hydrogen Energy. 45 (2020). https://doi.org/10.1016/j.ijhydene.2020.03.059.

[53] C. Zequine, C.K. Ranaweera, Z. Wang, P.R. Dvornic, P.K. Kahol, S. Singh, P. Tripathi, O.N. Srivastava, S. Singh, B.K. Gupta, G. Gupta, R.K. Gupta, High-Performance Flexible Supercapacitors obtained via Recycled Jute: Bio-Waste to Energy Storage Approach, Sci. Rep. 7 (2017) 1–12. https://doi.org/10.1038/s41598-017-01319-w.

[54] Y. Han, N. Shen, S. Zhang, D. Li, X. Li, Fish gill-derived activated carbon for supercapacitor application, J. Alloys Compd. 694 (2017) 636–642. https://doi.org/10.1016/J.JALLCOM.2016.10.013.

[55] M. Thommes, K. Kaneko, A. V. Neimark, J.P. Olivier, F. Rodriguez-Reinoso, J. Rouquerol, K.S.W. Sing, Physisorption of gases, with special reference to the evaluation of surface area and pore size distribution (IUPAC Technical Report), Pure Appl. Chem. 87 (2015) 1051–1069. https://doi.org/10.1515/pac-2014-1117.

[56] K.A. Cychosz, M. Thommes, Progress in the Physisorption Characterization of Nanoporous Gas Storage Materials, Engineering. 4 (2018) 559–566. https://doi.org/10.1016/J.ENG.2018.06.001.

[57] D.T. Bakhoum, K.O. Oyedotun, S. Sarr, N.F. Sylla, V.M. Maphiri, N.M. Ndiaye, B.D. Ngom, N. Manyala, A study of porous carbon structures derived from composite of cross-linked polymers and reduced graphene oxide for supercapacitor applications, J. Energy Storage. 51 (2022) 104476. https://doi.org/10.1016/j.est.2022.104476.

[58] B. Lu, J. Zhou, Y. Song, H. Wang, Molten-salt treatment of waste biomass for preparation of carbon with enhanced capacitive properties and electrocatalytic activity towards oxygen reduction †, (2016) 147–159. https://doi.org/10.1039/C5FD00215J.

[59] B. Szubzda, A. Szmaja, A. Halama, Influence of structure and wettability of supercapacitor electrodes carbon materials on their electrochemical properties in water and organic solutions, Electrochim. Acta. 86 (2012) 255–259.

https://doi.org/10.1016/J.ELECTACTA.2012.08.060.

[60] D. Chen, Z. Li, J. Jiang, J. Wu, N. Shu, X. Zhang, Influence of electrolyte ions on rechargeable supercapacitor for high value-added conversion of low-grade waste heat, J. Power Sources. 465 (2020) 228263. https://doi.org/10.1016/j.jpowsour.2020.228263.

[61] F. Barzegar, A.A. Khaleed, F.U. Ugbo, K.O. Oyeniran, D.Y. Momodu, A. Bello, J.K. Dangbegnon, N. Manyala, Cycling and floating performance of symmetric supercapacitor derived from coconut shell biomass, AIP Adv. 6 (2016). https://doi.org/10.1063/1.4967348.

[62] X. Han, H. Jiang, Y. Zhou, W. Hong, Y. Zhou, P. Gao, R. Ding, E. Liu, A high performance nitrogen-doped porous activated carbon for supercapacitor derived from pueraria, J. Alloys Compd. 744 (2018) 544–551. https://doi.org/10.1016/j.jallcom.2018.02.078.

[63] S. Sathyamoorthi, W. Tejangkura, M. Sawangphruk, Turning carbon-ZnMn2O4 powder in primary battery waste to be an effective active material for long cycling life supercapacitors: In situ gas analysis, Waste Manag. 109 (2020) 202–211. https://doi.org/10.1016/j.wasman.2020.05.007.